# Direct visualization of bacterial multispecies infection and symbiotic interactions within human bladder epithelial cells

Charlotte Abell-King[1], Alaska Pokhrel[1], Scott A. Rice[1,2],

Iain G. Duggin[1] & Bill Söderström[1,#]

[1] Australian Institute for Microbiology and Infection

University of Technology Sydney

Ultimo NSW, 2007, Australia

[2] Microbiomes for One Systems Health and Agriculture and Food, CSIRO

Westmead NSW, 2145

Sydney, Australia

# Address correspondence to:

Mail: Bill.soderstrom@uts.edu.au Tel: +61 02 9514 4970

**Summary**

Urinary tract infections (UTIs) are a worsening global health problem. Multispecies bacterial UTIs are common but are poorly recognized and understood. Here we developed host cell co-infection models combined with high resolution imaging to compare single- and multi-species infections with common uropathogens, uropathogenic *Escherichia coli* (UPEC), *Klebsiella pneumoniae* and *Enterococcus faecalis*. We demonstrate cooperation and direct interactions specifically between UPEC and *E. faecalis* within host cells that corresponded to an increased frequency of host cell infection. 3D imaging showed UPEC rods orientated perpendicular to the major host cell axis within single-species intracellular bacterial communities (IBCs), whereas UPEC cells often enveloped *E. faecalis* in multispecies IBCs. Furthermore, during dispersal from host cells, only the Gram-negative bacteria underwent infection-related filamentation (IRF) in multispecies infections. These first insights into intra-species synergies during UTIs at a single cell level should provide research pathways towards better diagnosis and treatment.

## Introduction

Urinary tract infections (UTIs) are amongst the most common bacterial infections globally (Antimicrobial Resistance, 2022). With an estimated 150 million people experiencing an UTI annually, they are the primary cause of GP visits (Flores-Mireles et al., 2015). Clinically, UTIs are normally attributed to only one species of bacteria at a time, with Uropathogenic *Escherichia coli* (UPEC) being the most commonly diagnosed infectious agent at a reported prevalence between 70 and 95% (Foxman, 2014; Klein and Hultgren, 2020; Kucheria et al., 2005; Shah et al., 2019; Xia et al., 2017). However at the same time, it is well established that there are a multitude of different bacterial species present in the bladder environment at any given time (Gaston et al., 2021), and it is known that in acute UTIs, polymicrobial infections are common, with both Gram-negative and Gram-positive pathogens present (Croxall et al., 2011; Stickler, 2008).

It has been observed indirectly that *Enterococcus faecalis* (a Gram-positive cocci) and UPEC are often associated with each other during outgrowth of cultures from UTIs (de Vos et al., 2017; Fourcade et al., 2015) and that *E. faecalis* can suppress the immune activation promoting UPEC virulence (Tien et al., 2017). However, multispecies UTI are clinically underdiagnosed, especially if they contain Gram-positive species (*e.g.*, enterococci), and are often disregarded as sample contamination (Kline and Lewis, 2016). An early study investigating UTIs from 80 female patients with cystitis found that UPEC was over twenty-fold more common than *E. faecalis* as the causative agent of the infections (Rosen et al., 2007). Conversely, another study found that when UPEC and *E. faecalis* were introduced simultaneously to urothelial cells that were shed from lower urinary tract symptom (LUTS) patients, only *E. faecalis* displayed cellular invasion while UPEC were found exclusively extracellular (Horsley et al., 2013).

70 These observations suggested that only one bacterial species would invade a given
71 bladder cell at a time, however those experiments were done under conditions where
72 *E. faecalis* had a much higher abundance than other species, including UPEC (Horsley
73 et al., 2013). While these studies suggest a difference in frequency of invasion
74 between Gram-negative and Gram-positive pathogens depending on different
75 environmental conditions (*e.g.,* varying urine flow rates), very limited information
76 regarding this event and the potential influence of co-existing bacteria on infection is
77 available at a single cell level.
78 Here we compared cellular invasion rates between continuous-flow and culture dish
79 UTI models, and used high-resolution fluorescence microscopy to determine whether
80 more than one species of bacteria would invade and form intracellular bacterial
81 communities (IBC) the same bladder cells, and, if so, whether or not they would
82 cooperate or compete for survival once intracellular. The pathogens used in this study
83 were Gram-negative Uropathogenic *Escherichia coli* (UPEC) and *Klebsiella*
84 *pneumoniae*, as well as the Gram-positive *Enterococcus faecalis,* as they are the three
85 most commonly found organisms in healthcare-associated UTIs (HAUTIs) (Tandogdu
86 et al., 2016), and are commonly co-isolated in clinical settings (Galvan et al., 2016),
87 especially in samples from catheter-associated urinary tract infections(Desai et al.,
88 2001; Ganderton et al., 1992; Macleod and Stickler, 2007; Wang et al., 2010).
89

90 **Results**

91 *Flow affects the invasion rates of the Gram-positive bacteria more than for the Gram-*
92 *negative bacteria.*
93 We established monospecies infections simulating uncomplicated UTIs using PD07i
94 human epithelial bladder cells, with either UPEC (strain UTI89 expressing cytoplasmic

95 mOrange2), *K. pneumoniae* (strain TOP52 expressing cytoplasmic mCerulean3) or *E.*
96 *faecalis* (strain SD234 expressing cytoplasmic GFP), to ascertain whether they were
97 capable of infecting host cells in a previously established *in-vitro* UTI flow-chamber
98 model and to establish base line infection rates (Iosifidis and Duggin, 2020;
99 Söderström et al., 2022). This model is based on a commercial flow-chamber system
100 (IBIDI $I^{0.2}$ $\mu$-Slides connected to NewEra syringe pumps) where constant flow is
101 applied throughout the infection cycle to simulate bladder flow. We also used a semi-
102 static infection model using 35 mm glass-bottom Petri dishes under constant shaking
103 (50 rpm), to determine differences in invasion rates between situations of constant
104 flow and circular agitation. In both models, the bladder cells were exposed a total
105 ~ $10^7$ cells of each bacterial species, as routinely done in murine models (Rosen et al.,
106 2008; Tien et al., 2017). All three pathogens invaded the epithelial bladder cells both
107 in the flow-chamber and Petri-dish conditions (Figure 1A - C).

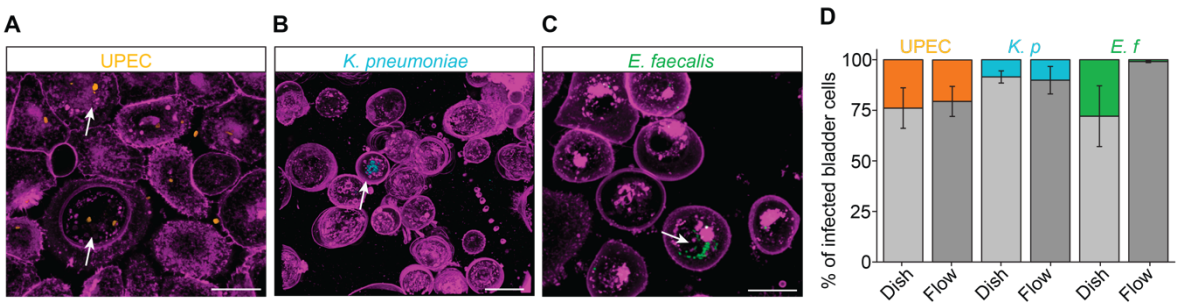


108

109 *Figure 1. Single-species model infections using Gram-negative and Gram-positive*
110 *uropathogens.*
111 *PD07i human epithelial bladder cells (cytoplasmic membranes labelled with*
112 *CellBright650, magenta) grown on a 35-mm glass bottom petri-dish or in a flow*
113 *chamber were infected by either* ***A****, UPEC (UTI89 expressing cytoplasmic mOrange2);*
114 ***B****,* K. pneumoniae *(TOP52 expressing cytoplasmic mCerulean3); or* ***C****,* E. faecalis
115 *(SD234 expressing cytoplasmic GFP). White arrows indicate internalised bacteria.* ***D****,*

116 *Proportion of bladder cells infected (colour) and uninfected (grey) in various conditions*
117 *and bacterial species. K. p* = K. pneumoniae*. E. f* = E. faecalis*. Dish = 35 mm glass*
118 *bottom petri-dish. Flow* = 15 μl $min^{-1}$ *in flow chamber (IBIDI μ-Slide $I^{0.2}$). Scale bars =*
119 *20 μm.*
120
121 At 20 h post inoculation, UPEC had invaded the most bladder cells of the tested Gram-
122 negative species (23.9 ± 10% of the bladder cells in the semi-static petri dish model
123 and 20.5 ± 7.4% in the flow model, Mean ± S.D., n > 432 from 3 infection experiments),
124 while *K. pneumoniae* only invaded approximately half of this number (8.49 ± 3% in the
125 dish model and 10.1 ± 6.8 % in the flow model, n > 321 from 3 infections of each
126 condition) (Figure 1D). On average 27.9 ± 15% of the bladder cells contained
127 intracellular *E. faecalis* in the dish model (n = 335, from 3 experiments) (Figure 1D).
128 In contrast, *E. faecalis* invaded less than 1% of the bladder cells under the flow-
129 chamber conditions (n = 462, from 3 independent experiments).
130
131 *The Gram-negative bacteria were predominantly organised vertically in IBCs.*
132 Upon closer inspection of Gram-negative IBCs, the peripheral bacterial cells showed
133 a tendency to orientate perpendicular to the xy-plane, with the overall IBC shape
134 resembling an irregular sphere (Figure2A – D). A similar IBC structure has been
135 observed for UPEC IBCs harvested from mice bladders (Justice et al., 2004), where
136 many of the bacteria were also reported as coccoid in shape. Since those observations
137 (Justice et al., 2004), were made using 2D microscopy there may have been an
138 overestimation of the amount of coccid shaped cells; 3D microscopy results confirmed
139 that vertically oriented rod cells appear roundish in 2D projections (Figure 2B, 2D and
140 2F).

141 It has been observed that some intracellular bacteria do not grow into large IBCs but
142 remained in small clusters over time (Figure 2E) (Justice et al., 2004). Similar to larger
143 IBCs, we found that the individual cells in the clusters and small IBCs predominantly
144 were oriented vertically (Figure 2F). These non-growing clusters of cells and
145 transiently stalled IBCs, reminiscent of quiescent intracellular reservoirs (QIRs), are
146 seemingly protected from the effects of antibiotics and appears undetected by the host
147 cell immune system (Mulvey et al., 2001; Mysorekar and Hultgren, 2006). These small
148 IBCs were always encapsulated by membrane (Figure 2G). Inspecting confocal Z-
149 stacks we observed multiple distinct UPEC IBCs encapsulated clusters in single
150 bladder cells (Figure 2G). Other bacteria have been found in cellular cavities and
151 encapsulated by internal membranes during invasion in model infection systems
152 suggesting that this is a general feature (Prudent et al., 2021).

153 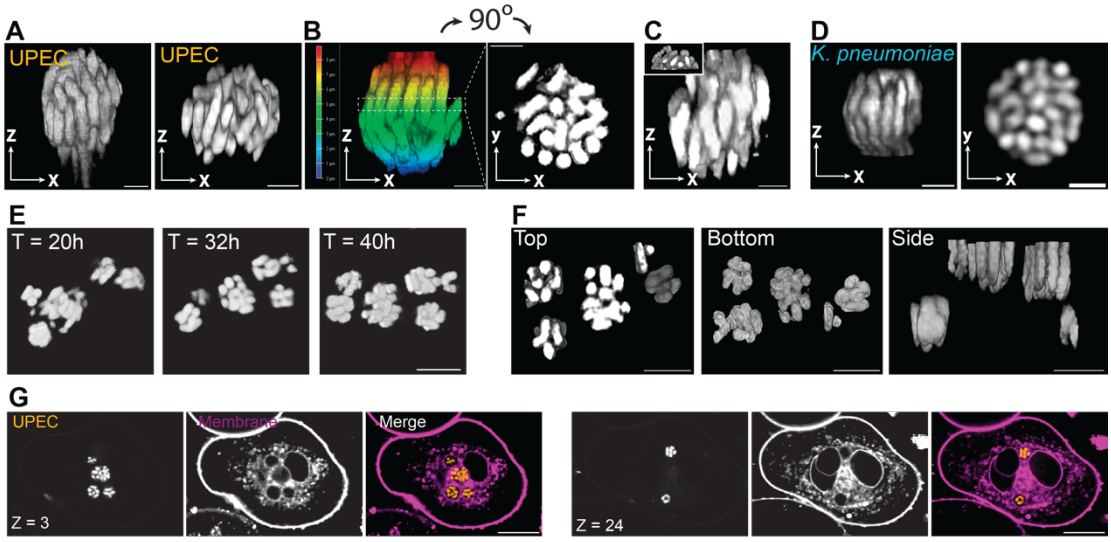


154 *Figure 2. Structure of Gram-negative intracellular bacterial communities.*

155 ***A**, Cellular orientation of UPEC in IBCs. The cells tend to organise vertically at the*
156 *periphery of an IBC. **B**, Depth coded 3D reconstruction of an UPEC IBC. A cut out*
157 *(dotted lines) section turned 90° is shown to the right. **C**, An IBC cut optically in half to*
158 *show orientation of internal bacteria. Most internally localised UPEC cells orient*

159 *vertically to the xy-plane when in IBCs. Inset show x-y view of the same 3D*
160 *reconstruction.* ***D****, 3D reconstruction (left) and 2D confocal image (right) of K.*
161 *pneumoniae IBCs. Cells organise vertically at the periphery of the IBCs.* ***E****, Multiple*
162 *UPEC clusters not expanding over time. T indicates time since inoculation. Note cells*
163 *are alive and thus move intracellularly between time points.* ***F,*** *Cellular clusters and*
164 *small IBCs orient vertically when intracellular.* ***G,*** *Two distinct planes from a Z-stack*
165 *taken from a single cell at T = 40 h (post inoculation) showing multiple UPEC IBCs*
166 *localized in membrane pockets. Distance between consecutive Z planes was* $\Delta Z$ *=*
167 *0.250* $\mu$*m. Scale bars A - D and F = 2* $\mu$*m. Scale bar E = 4* $\mu$*m. Scale bar G = 10* $\mu$*m.*
168
169 *Elevated infection rates for UPEC in dual species infection with* E. faecalis*.*
170 Because very few bladder cells were infected by *E. faecalis* in the flow-chamber model,
171 the culture-dish model was used to study multispecies UTIs (mUTIs). We co-
172 inoculated the bladder cells with equal numbers of UPEC and *E. faecalis* (a combined
173 total of ~ $10^7$ bacteria (Tien et al., 2017)). Based on images of more than 560 randomly
174 inspected bladder cells (regions of interest [ROIs] were chosen based on fluorescence
175 signal from bladder cell membranes) from three independent experiments, almost half
176 (~ 45%, Figure 3B) were invaded by at least one type of bacterial species. Most
177 infected bladder cells were only invaded by one species (Figure 3A, arrows).
178

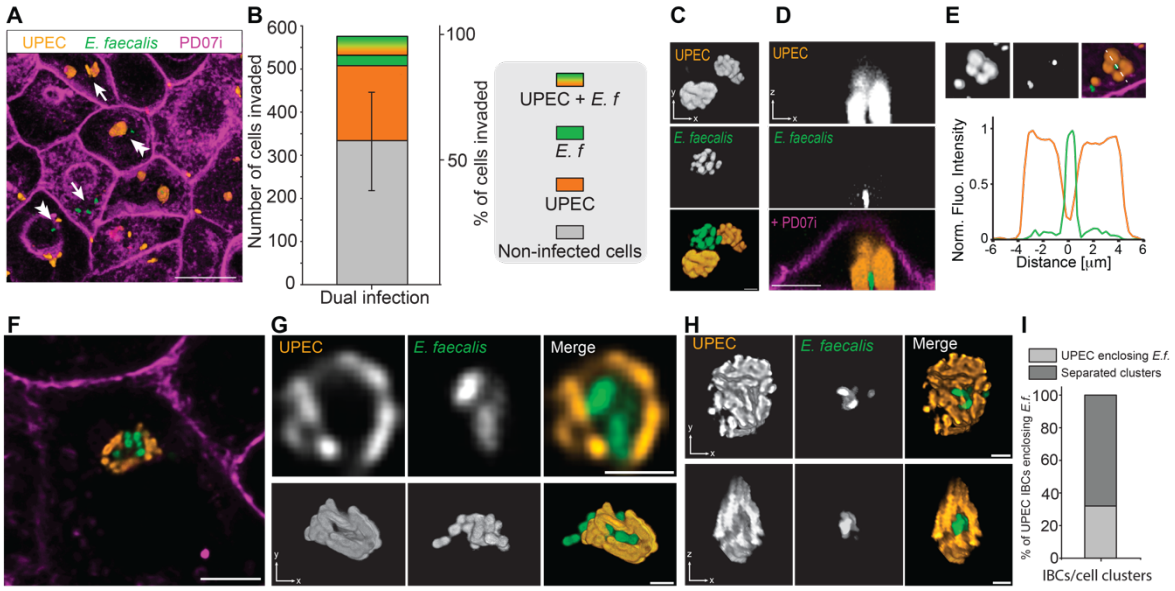


179

180 *Figure 3. Increased bladder cell invasion during* UPEC *and* E. faecalis *coinfections.*

181 ***A**, PD07i (membranes labelled with CellBright 405 or 650) cells co-infected with* UPEC

182 *(orange) and* E. faecalis *(green). Scale bar 20 = µm.* ***B**, ratio of invaded PD07i cells.*

183 *E. f = E. faecalis* ***C**, Typical intracellular* UPEC *(orange) and* E. faecalis *(green) clusters.*

184 UPEC *appeared more tightly packed than* E. faecalis. *Scale bar 1 µm.* ***D** and **E**, Low*

185 *resolution Z-stacks showing UPEC surrounding* E. faecalis *in dual-infected PD07i cells.*

186 *The graph in E shows fluorescence intensity traces for the white dash line in the image*

187 *above. UPEC (orange) and* E. faecalis *(green).* ***F**, **G** and **H**, Representative images*

188 *and confocal 3D reconstructions of* E. faecalis *(green) surrounded by UPEC (orange).*

189 *Scale bar **F** = 10 µm. Scale bars **G**, **H** = 2 µm.* ***I**, Percentage of dual invaded PD07i*

190 *cells with UPEC cells enclosing* E. faecalis cells *(as shown in **H**). Note various*

191 *orientations of reconstructed Z-stacks.*

192

193 In these dual-species infections, UPEC was internalised in 33% of cells, whereas

194 *E. faecalis* was internalised in only 4% (Figure 3B). Interestingly, a relatively high

195 number, 44 of 564 or approximately 8% of the bladder cells were invaded by both

196 bacterial species at the same time (Figure 3A, arrow heads). While the percent of
197 bladder cells invaded by *E. faecalis* alone decreased roughly 7-fold compared to the
198 single-species infection (Figure 1), the overall percentage of invasions during dual-
199 species infections increased to almost 45% (43.6 ± 19.3% (n = 564 cells, from 3
200 experiments)), suggesting a cooperative regulation and symbiosis.
201 As noticed for single species infections, the arrangement of the internalised bacteria
202 was distinct for each species; UPEC formed condensed IBCs while *E. faecalis* were
203 often individual cells or in loosely organised clusters in which single cells were readily
204 resolved (Figure 3C). Remarkably, in co-infected cells we noticed that UPEC was often
205 closely associated with *E. faecalis* (Figure 3D - F). With increased resolution, it
206 became clear that tightly packed UPEC cells formed multicellular communities that
207 frequently surrounded one or a few *E. faecalis* cells (Figure 3G - H). UPEC
208 encapsulation of the *E. faecalis* cells was evident in 32% of all bladder cells with dual
209 species invasion (Figure 3I). We speculate that this observation strengthens the notion
210 that *E. faecalis* enhances *E. coli* invasion and intracellular proliferation to collectively
211 increase the likelihood of prolonged infection (Tien et al., 2017).
212
213 K. pneumoniae *decreases the overall infection rates of bacteria in dual and multi-*
214 *species infections.*
215 To investigate whether other species would coinfect the PD07i cells and exhibit similar
216 interactions as seen above, we carried out experimental infections with other
217 combinations of bacteria, *E. faecalis* and *K. pneumoniae* (Gram-positive/Gram-
218 negative pair), UPEC and *K. pneumoniae* (Gram-negative/Gram-negative pair) or all
219 three species. We detected host cells containing all combinations of the bacteria

220 investigated (Figure 4A – C), but the intracellular arrangement and frequencies of the

221 infecting bacteria varied substantially.

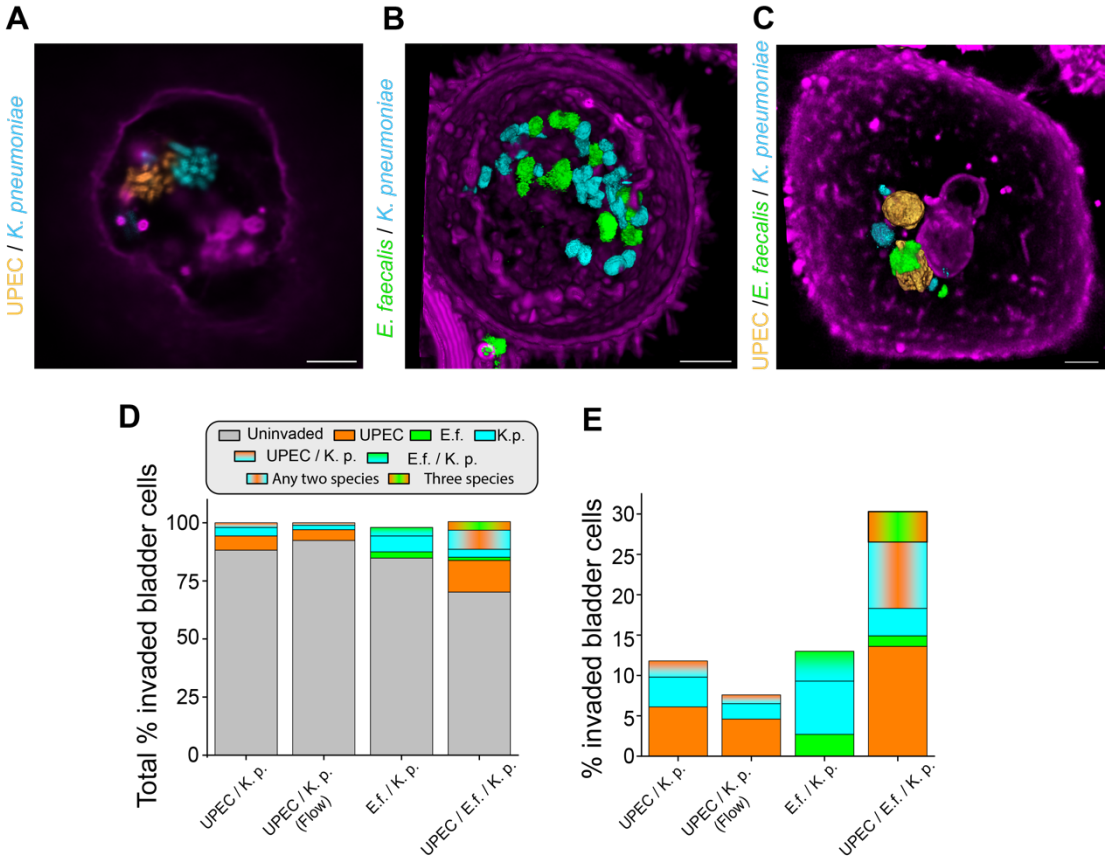


222

223 *Figure 4. Prevalence of bacterial invasion during dual- and triple-species infections.*

224 *Representative PD07i cells invaded by* ***A****,* UPEC and K. pneumoniae *(2D confocal*

225 *image);* ***B****,* E. faecalis *and* K. pneumoniae *(deconvolved 3D-reconstruction of a*

226 *confocal Z-stack); and* ***C****,* UPEC, E. faecalis and K. pneumoniae *(deconvolved 3D-*

227 *reconstruction of a confocal Z-stack). PD07i membranes labelled with CellBright 650.*

228 *Scale bars = 4 μm.* ***D****, Percentage of invaded bladder cells.* UPEC and/or

229 K. pneumoniae *invaded 11.8 (± 9) % of PD07i cells in dishes and 7.6 (± 2) % in flow.*

230 E. faecalis *and* K. pneumoniae *invaded 12.8 (± 8) % of PD07i cells in dishes.* UPEC,

231 E. faecalis *and* K. pneumoniae *together invaded 29.8 (± 10.3) % of PD07i.* ***E****,*

232 *Distribution of species in invaded bladder cells. E. f* = E. faecalis. *K. p* = K. pneumoniae.

233

234 In contrast to the UPEC / *E. faecalis* case, encapsulation was not observed when *E.*
235 *faecalis* was co-infected with *K. pneumoniae,* nor when the two Gram-negative
236 species (*i.e.* UPEC and *K. pneumoniae)* were co-inoculated. UPEC and *K.*
237 *pneumoniae* often formed dense IBCs adjacent to one another but did not mix with
238 each other (Figure 4A). In the case of *E. faecalis* and *K. pneumoniae* we noticed that
239 while they were capable to co-invade bladder cells, they did not form dense IBCs and
240 were largely spread out inside the bladder cells (Figure 4B). *E. faecalis* has previously
241 been shown to antagonize *K. pneumoniae* biofilm formation during mixed growth albeit
242 under different settings to the intracellular conditions in present study (Ballen et al.,
243 2020). For three species infections (UPEC, *E. faecalis* and *K. pneumoniae)*, the UPEC
244 / *E. faecalis* pair again showed similar organizational patters as they did in two species
245 infections, while *K. pneumoniae* was predominately localized separate from the other
246 two (Figure 4C).
247
248 Based on 4 independent infection experiments (n > 100 for each) performed in the 35
249 mm dishes, UPEC and *K. pneumoniae* coinfected 2% bladder cells (Figure 4D - E).
250 When running UPEC and *K. pneumoniae* together in the flow channel model each
251 species invaded around 5 % of the bladder cells (combined did UPEC and *K.*
252 *pneumoniae* invade 11.8 ± 0.9%), while more than in the static model, a significant
253 reduction from the single species infection situation (Figure 4D - E). This suggests a
254 possible competition between UPEC and *K. pneumoniae* when they are together in a
255 UTI environment. The total percentage of invaded bladder cells in a *E. faecalis* and *K.*
256 *pneumoniae* dual species combination was ~ 13%, with 3.7% of all observed of
257 bladder cells invaded by both (n = 463 cells from 4 independent experiments). Finally,
258 in the three species infections roughly 30% of bladder cells were invaded by at least

259 one species, with 3.7% invaded by all three (Figure 4D - E). This was less than the
260 invasion rate in UPEC / *E. faecalis* dual infections where ~ 45% of the bladder cells
261 were invaded (Figure 3B), again suggesting that *K. pneumoniae* has an inhibitory
262 effect on invasion efficiency during multi-species infections.
263
264 *Gram-negative bacteria undergo infection-related filamentation, while Gram-positive*
265 *do not.*
266 During murine model UTIs, UPEC have been seen to undergo morphological changes
267 during intracellular bacterial community (IBC) formation and dispersal, where UPEC
268 grow into long filamentous cells (Justice et al., 2006). These morphologies were later
269 also seen in female patents with cystitis (Rosen et al., 2007) and more recently also
270 confirmed in flow-chamber models using human bladder cells and urine (Andersen et
271 al., 2012; Iosifidis and Duggin, 2020; Klein et al., 2015; Söderström et al., 2022). To
272 determine whether single or multi-species infections undergo the same morphological
273 changes under the established conditions, we next visualized cells sampled after the
274 dispersal stage of infection by exposing infections to human urine (~20 h) (Iosifidis
275 and Duggin, 2020; Söderström et al., 2022). Both UPEC and *K. pneumoniae* formed
276 filaments of several hundreds of microns long (Figure 5A - B). For *K. pneumoniae*,
277 similar morphology cycles have been previously observed in murine models (Rosen
278 et al., 2008), but not in *in-vitro* models using human bladder cells and urine. The
279 average length of *K. pneumoniae* filaments from infections in petri dishes was 47.3 ±
280 45.3 μm (n = 98) and 54 ± 57.8 μm (n = 156) in flow-chambers. For UPEC was the
281 average length of the filaments 56.0 ± 59.9 μm (n = 158) and 43.3 ± 40.05 μm (n =
282 122) in dishes and flow-chambers, respectively (Figure 4D). By comparison, UPEC
283 and *K. pneumoniae* rods grown in LB medium were on average 3.46 ± 0.69 μm (n =

187) and 3.62 ± 0.76 μm (n = 192), respectively (Figure 5D). We classified cells filaments if they are two times the average WT cell length, *i.e.*, 7 μm. It is worth noting that the percentage of cells that underwent filamentation (but not the average length of filaments) was lower in the dish model compared to the flow-chamber model, suggesting that proficiency of morphology changes is connected to flow and shear-force dynamics (Andersen et al., 2012).

In contrast to the Gram-negative species, and as expected, *E. faecalis* did not filament upon exposure to human urine (Figure 4C), average lengths after an infection were 1.42 ± 0.4 μm (n = 215) from petri-dish infection and 1.59 ± 0.41 μm (n = 102) from flow chambers which was marginally shorter than lengths for *E. faecalis* cells grown in BHI medium only (1.74 ± 0.31 μm (n = 238)) (Figure 5D). Similar results for filamentation were observed during mixed infections (Figure 5E). Overall, this shows that infection-related filamentation is a broadly occurring phenomenon as it also transpire during multispecies infections.

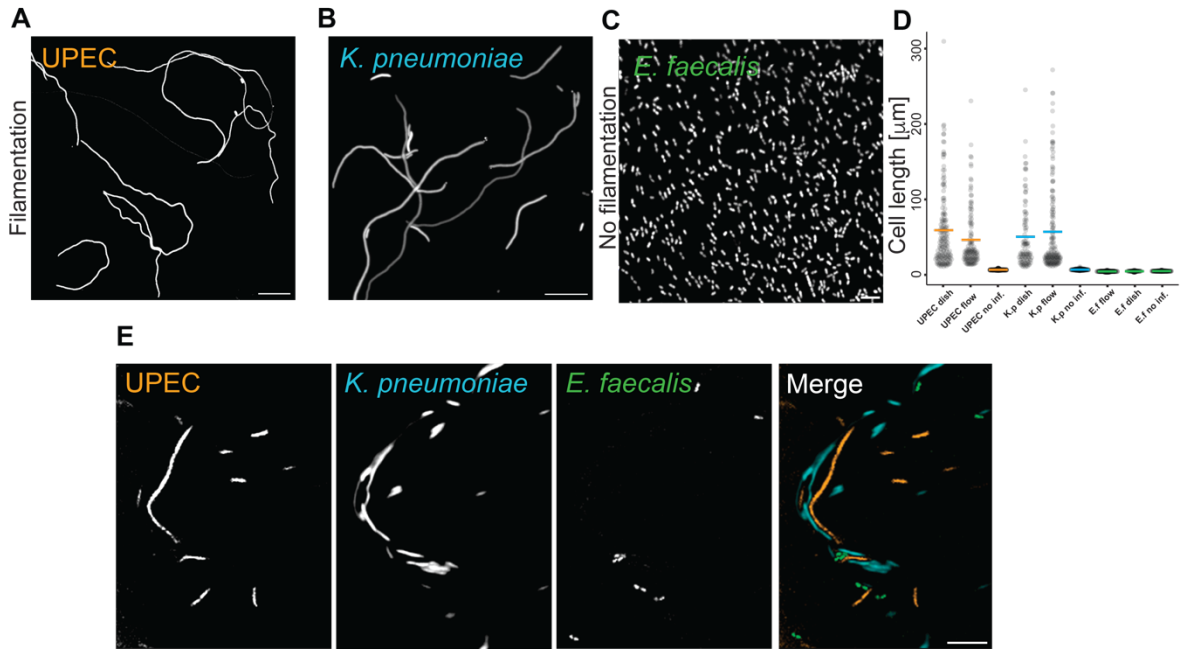

300 *Figure 5. Gram-negative, but not Gram-positive, species undergo infection-related*
301 *filamentation in both single and multi-species infections.*
302 *Representative images of bacteria after being exfoliated from PD07i cells during single*
303 *species infections.* ***A****,* UPEC*,* ***B****,* K. pneumoniae ***C****,* E. faecalis*.* ***D****, Average lengths of*
304 *bacterial filaments* (UPEC and K. pneumoniae*) and cells* (E. faecalis*) after 20 h of*
305 *urine exposure during infections. The average length of UPEC filaments was 56.0 ±*
306 *59.9 μm (n = 158) in dishes, and 43.3 ± 40.05 μm (n = 122) in flow.* K. pneumoniae
307 *filaments were 47.3 ± 45.3 μm (n = 98) in dishes and 54 ± 57.8 μm (n = 156) in flow*
308 *and. UPEC and* K. pneumoniae *rods grown in LB media were on average 3.46 ± 0.69*
309 *μm (n = 187) and 3.62 ± 0.76 μm (n = 192), respectively. Average lengths of* E. faecalis
310 *after an infection were 1.42 ± 0.4 μm (n = 215) from petri-dish infection and 1.59 ±*
311 *0.41 μm (n = 102) from flow chambers. Lengths for* E. faecalis *cells grown in BHI*
312 *media only was 1.74 ± 0.31 μm (n = 238). Dish = 35-mm glass bottom petri-dish. Flow*
313 *= 15 μl min$^{-1}$ in flow chamber (IBIDI I$^{0.2}$).* ***E****, Filamentation of UPEC and* K. pneumoniae
314 *but not* E. faecalis *during three species infections. Scale bars* ***A****,* ***B*** *and* ***E*** *= 10 μm,* ***C***
315 *= 4 μm.*
316
317 Discussion
318 We have established a set of multi-species urinary tract infection models. We visually
319 compared invasion frequencies of three common urinary tract pathogens,
320 Uropathogenic *Escherichia coli*, *Klebsiella pneumoniae* and *Enterococcus faecalis,*
321 using a human bladder cell *in-vitro* infection model under two different conditions ('flow'
322 and 'dish'). UPEC showed highest overall invasion frequency, followed by *K.*
323 *pneumoniae*. *E. faecalis* predominantly invaded bladder cells only in the culture dish
324 model. UPEC and *K. pneumoniae* invasion frequency were only marginally impacted

325 by switching from continuous flow to circular agitation. Differences in invasion
326 frequency between UPEC and *K. pneumoniae* has been observed previously in
327 murine models, and has been attributed differences in adhesion capabilities through
328 lower type 1 pilus expression (Rosen et al., 2008). *E. faecalis* exhibited a large
329 variation in invasion frequency between the models tested in this study. While *E.*
330 *faecalis* is a well-established uropathogen (Ch'ng et al., 2019; Garsin et al., 2014), our
331 observations suggest a weakened ability to adhere and invade bladder cells under the
332 relatively higher flow conditions in our model. At this point we do not fully understand
333 the molecular details resulting in the large variation in bladder cell invasion of
334 *E. faecalis* between our flow and dish models, but similar behaviours have previously
335 been linked to the reduced adherence capabilities of *E. faecalis* (Ch'ng et al., 2019;
336 Kau et al., 2005; Kline and Lewis, 2016; Shankar et al., 2001).
337 UPEC bladder cell invasion has been extensively studied and its efficiency depends
338 on type-1 fimbriae (*fim* operon genes, e.g. *fimH* for adhesion) and specific bacterial
339 lipopolysaccharide O-antigen (WaaL) expression as well as TLR4 signalling
340 mechanisms within the host cells (Billips et al., 2007; Billips et al., 2008; Duncan et al.,
341 2004; Eto et al., 2007; Martinez et al., 2000; Mulvey et al., 1998; Song et al., 2007).
342 The overall higher rate of invaded bladder cells from all tested bacterial species in the
343 dish model was somewhat surprising as FimH has previously been shown increase
344 the binding affinity during flow induced stress in model systems and molecular
345 dynamics simulations (Sauer et al., 2016). In our experimental system the cells
346 experience overall less stress in the dishes and there is less sheer force to compete
347 against compared to in a constant flow. In our model geometry using 15 µl $min^{-1}$ flow
348 rate and dynamic viscosity of 0.0072 dyn * s * $cm^{-2}$ results in a shear stress of $\tau$ =

349 0.055 dyn $cm^{-2}$ and shear rate of ~ 7.64 $s^{-1}$, this is higher than in other *in-vitro* flow
350 models simulating a resting bladder (Andersen et al., 2012).
351
352 Overall, the vertical orientation of cells within Gram-negative IBCs is in contrast to
353 previous observations of subcellular bacterial organization in environmental biofilms
354 where peripheral cells tend to orient with the xy-plane and internally located cells orient
355 vertically due to mechanical forces (Qin et al., 2020; Yan et al., 2016), and it was found
356 that shorter cells produced a higher degree of verticalization of the biofilms (Beroz et
357 al., 2018). It should be noted that while these studies focused on *Vibrio cholerae*
358 growing on a surface, *V. cholerae* are similar in shape to UPEC and *K. pneumoniae*
359 and from a purely physical viewpoint it would therefore stand to reason that they would
360 produce biofilms of comparable geometrical dimensions. One possibility is that the
361 dissimilarity in biochemical composition and intracellular space constraints are instead
362 the main drivers for the difference in cellular orientation and architecture between IBC
363 growth and externally grown biofilms (Flemming and Wingender, 2010).
364
365 In our multispecies infection experiments, we demonstrated cooperation, here defined
366 as overall increased invasion frequency, between UPEC and *E. faecalis* at a single
367 cell level using fluorescence microscopy. While details governing intracellular
368 coexistence of bacteria during UTIs remains elusive, our results indicate that
369 whenever UPEC and *E. faecalis* are introduced together the overall rate of infection
370 increases on the expense of *E. faecalis* alone infections. Similar cooperation and
371 increase in pathogenicity by UPEC and *E. faecalis* have been indirectly demonstrated
372 in murine models (Tien et al., 2017). This commensalism is not universal however,
373 whenever *K. pneumoniae* was introduced into a multispecies infection situation was

374 the average invasion frequency always lower than in the corresponding single species
375 infections. *E. faecalis* has previously been implicated in suppressing *K. pneumoniae*
376 growth during polymicrobial biofilm formation in human urine (Ballen et al., 2020). This
377 suppression by *E. faecalis* seems also be extended to other Gram-negative species
378 (*i.e.*, *Pseudomonas aeruginosa*) (Zhu Tan et al., 2022). All data taken together
379 suggests that the effect of introducing additional species in a UTI does not have a
380 linear accumulative effect on invasion frequencies but is rather governed by specific
381 biochemical responses of the particular species present.
382 We hope that the data presented in this study initiate a spark for further investigation
383 into detailed genetics studies exploring dedicated signalling pathways in multispecies
384 UTIs at a single cell level as this will undoubtably play an increasingly important role
385 in understanding competing or cooperative behaviours of bacteria during infections as
386 antimicrobial resistance continue to rise.
387

388 **Materials and Methods**

389

390 **Human Ethics**

391 This study was approved by the UTS Human Research ethics committee with approval
392 numbers HRCH REF No. 2014000452 and HREC ETH22-7590. All urine doners gave
393 their approval to participate in this study by informed consent under this study's ethics
394 approval number above.

395

396 **Plasmid construction**

397 pCAK1 and pAP1 plasmids were constructed by replacing the GFP sequence in pGI5
398 (Iosifidis and Duggin, 2020) with mCerulean3 and mOrange2 sequences, respectively.
399 The mCerulean3 and mOrange2 gene fragments were amplified from pEB1-
400 mCerulean3 and mOrange2-pBAD plasmids, both obtained from Addgene (Addgene
401 plasmids #103973 and #54531) (Balleza et al., 2018; Shaner et al., 2008). To
402 construct pCAK1 and pAP1, pGI5 was digested with *Nco*I and *Bam*HI, and assembled
403 with mCerulean3 and mOrange2 PCR products containing 20-30 bp homologous
404 regions from pGI5 on both the ends. This was performed using a *in vivo* DNA assembly
405 method (Watson and Garcia-Nafria, 2019). The final products were confirmed by
406 Sanger sequencing and fluorescence microscopy.

407

408 **List of Primers**

| | |
|---|---|
| mCerulean3_FW | GCC CGG TCT AGA GGA GGT ACT ACC ATG AGT AAA GGA GAA GAA CTT TTC ACT |
| mCerulean3_RV | GGT CGA CGG ATC TTT AGG ATC CTT TTA TTT GTA TAG TTC ATC CAT GCC ATG |

| | |
|---|---|
| mOrange2_FW | CGG TCT AGA GGA GGT ACT ACC ATG GTG AGC AAG GGC GAG GAG |
| mOrange2_RV | CAG GTC GAC GGA TCT TTA GGA TCC TTA CTT GTA CAG CTC GTC CAT GCC |

409

410 **Bacterial growth**

411 Bacterial strains were used as follows: Uropathogenic *Escherichia coli* UTI89
412 transformed with mOrange2 (pAP1) or mCherry (pGI6) (Wright et al., 2021), *Klebsiella*
413 *pneumoniae* TOP52 transformed with mCerulean3 (pCAK1) or sfGFP (pGI5), and
414 *Enterococcus faecalis* OG1RF expressing GFP from the chromosome (Debroy et al.,
415 2012). All fluorescent proteins were produced as constitutively expressed freely
416 diffusing molecules in the cytoplasms of the corresponding strain. A single colony of
417 respective bacterial strain was grown overnight in a 20 ml Luria Broth (*E. coli* and *K.*
418 *pneumoniae*) or Brain Heart Infusion (*E. faecalis*) culture at 37°C without shaking to
419 induce expression of type-1 pili which facilitates adhesion to the bladder cells during
420 infection. Antibiotics were added when needed (Spectinomycin 50 µg $ml^{-1}$, Rifampicin
421 100 µg $ml^{-1}$). The following morning, the cultures were pelleted and resuspended in 1
422 x PBS added to the infection model.

423

424

425

426

427

428

429

430 *Table 1: Bacterial species used in this study*

| Species | Strain | Fluorescent Protein | Plasmid Or Chromosome | Source |
|---|---|---|---|---|
| *E. faecalis* | OG1RF | GFP | Chromosome | Prof. Garsin (Uni Texas) |
| *UPEC* | UTI98 | mOrange2 | Plasmid (pAP1) | Lab strain |
| *UPEC* | UTI98 | mCherry | Plasmid (pGI6) | Lab strain |
| *K. pneumoniae* | TOP52 | mCerulean3 | Plasmid (pCAK1) | Prof. Hultgren (Uni Washington) |
| *K. pneumoniae* | TOP52 | sfGFP | Plasmid (pGI5) | Prof. Hultgren (Uni Washington) |

431

432 **Bladder cell growth**

433 Immortalized Epithelial bladder cells (PD07i (Berry et al., 2009; Klumpp et al., 2001))
434 were grown and maintained in EPILIFE media supplemented with Human
435 Keratinocyte Growth supplement (HKGS) in 5% $CO_2$ at 37 °C. Cells were split as
436 required using standard Trypsinization methods upon reaching 80% confluency.

437

438 **Human urine preparation**

439 Human urine was collected from both male and female donors. Samples were
440 collected in the mornings and stored at 4 °C for at least 2 days before further
441 processing. Samples were pelleted at 3000 rpm, the supernatant filtered through a 0.2
442 μm filter and aliquoted into 50 ml falcon tubes before placed in – 20 °C for storage
443 until use. Urine was only used if the pH was between 5-6.5 and the Urine Specific
444 Gravity (USG) was in the range between 1.024 to 1.030, values that has been shown

445 to produce high degree of filamentation (Iosifidis and Duggin, 2020; Söderström et al.,
446 2022).
447
448 **Infection models**
449 The *in-vitro* UTI flow channel models have been described previously (Andersen et al.,
450 2012; Iosifidis and Duggin, 2020). Briefly, μ-Silde $I^{0.2}$ Luer (IBIDI #80166) flow
451 channels were seeded with bladder cells according to the manufacturer's
452 recommendations. The channels were connected to a New Era pump system for
453 continuous flow of nutrients, this was left to run until a confluent layer of bladder cells
454 formed (Söderström et al., 2022). Bacterial cells resuspended in PBS at an $OD_{600}$ of
455 0.2 - 0.4 were introduced fully in the flow channels and flushed at a flow rate of 15 μl
456 $min^{-1}$ for 10-15 minutes (resulting in a total of ~$10^7$ bacterial cells run over the bladder
457 cells depending on concentration and species, as determined by CFU counts. For the
458 dish models the total amount of bacteria (~$10^7$) was distributed evenly over the bladder
459 cells at one time point only), before fresh EPILIFE media again was flown over the
460 cells for 7 hours to allow for invasion. After this, the media was exchanged to EPILIFE
461 containing antibiotics (Gentamycin and Ampicillin, f.c. 200 μg $ml^{-1}$) for 13 hours to
462 eliminate all extracellular bacteria. To monitor formation of intracellular bacterial
463 communities, channels were taken to the microscope for imaging at this point.
464 To generate filaments, after subjecting samples to the EPILIFE/antibiotics mixture,
465 human urine was added to the flow system (15 μl $min^{-1}$) for 20 hours. Bacterial
466 samples were collected through the back-end of the flow channels, washed once in 1
467 x PBS, resuspended in LB or BHI. 4 μl of respective cultures were placed on 2 %
468 agarose pads (w/w) and directly taken for imaging. In the semi-static infection model
469 the same experimental workflow was followed with the same time intervals in changing

470 media, with the exception that all steps were carried out in a 35 mm Petri dish (IBIDI
471 glass bottom dish with glass coverslip bottom (#1.5), pre-sterilized, cat number
472 #81218-200) placed in a $CO_2$ incubator at 37 °C with 50 rpm shaking (instead of
473 continuous flow). To generate filaments in the Petri dish model, 1 ml urine was added
474 and manually exchanged for the first 4-5 hours before a final resuspension of 3 ml was
475 done and left in the incubator for 15 hours. In the static model, just prior to imaging
476 were bladder cell membranes stained with CellBrite405 or 650 in PBS (f.c. 1:100, with
477 the addition of CellBrite Enhancer to mask intracellular fluorescence according to the
478 manufacturer's recommendations) for 40 minutes, washed twice and again covered
479 with EPILIFE to sustain cell health during imaging.
480
481 **Imaging**
482 Imaging was performed on a Leica Stellaris confocal microscope equipped with a 63x
483 oil objective enclosed in an environmental chamber operated at 37 °C and 5 % $CO_2$
484 (Oko-Lab). The fluorophores were excited by a white laser at optimized wavelengths,
485 and emission was collected in pre-set system optimised detector intervals for
486 AlexFluor405, mCerulean3, EGFP, mOrange2 and AlexaFluor647 depending on
487 experiment, to minimize channel crosstalk. Z-stacks were captured to validate that the
488 bacteria in fact were inside the blabber cells. Image size was either 2048 x 2048 or
489 4096 x 4096, with pixel size 90 and 45 nm, respectively. The pinhole was set to 1 AU
490 and Z-stacks were collected with software optimized step length of either 125 or 250
491 nm (30-99 images per stack, depending on step length and thickness of the bladder
492 cells). Reconstruction and deconvolution of Z-stacks were performed in the Leica LAS
493 software or in FIJI (ImageJ).
494

495 **Quantification and statistical analysis**

496 Raw microscopy images, deconvoluted Z-stacks and movies were transferred to FIJI
497 (ImageJ) for final analysis and processing. Fluorescence traces were analysed in
498 OriginPro 2021 (V. 9.8.0.200 [Academic]). Note that all fluorescence traces were
499 generated from raw microscopy data and not deconvoluted data. Cell lengths were
500 extracted from MicrobeJ (rod and cocci) (Ducret et al., 2016) or by manual tracing in
501 Fiji (filaments). Averages and errors bars in plots from multispecies infection represent
502 the overall change in infections regardless of what species that contributed to the
503 change. Evaluations of statistical significance were performed using students T-tests
504 using GraphPad Prism software (v.9.2). Levels of significance are indicated as follows:
505 ns, not significant; *, $P < 0.05$; **, $P < 0.01$; ***, $P < 0.001$;****, $P < 0.0001$.

506

507 **Data availability**

508 - Data reported in this paper will be shared by the lead contact upon request.
509 - This paper does not report original code.
510 - Any additional information required to reanalyse the data reported in this
511 paper is available from the lead contact upon request.

512

513 **Acknowledgments**

514 The authors want to thank Prof. Danielle Garsin (University of Texas) for the *E. faecalis*
515 OG1RF strain and Prof. Scott Hultgren (University Washington in St. Louis) for the *K.*
516 *pneumoniae* TOP52 strain. This study received funding from internal UTS and
517 Australian Institute for Microbiology and Infection (AIMI) funding schemes to S.R. and
518 B.S. The authors acknowledge the use of the Stellaris confocal microscope in the

Microbial Imaging Facility at AIMI in the Faculty of Science, the University of Technology Sydney.

**Author contributions**

B.S. conceptualised the study, and conduced the experiments together with C.A-K. C.A-K and A.P constructed plasmids. I.D., C.A-K and B.S. analysed the data. S.A.R. and B.S. raised funding from UTS and AIMI for this project. All authors contributed to the manuscript (writing and editing) and approved the final version.

530 **References**
531


532 Andersen, T.E., Khandige, S., Madelung, M., Brewer, J., Kolmos, H.J., and Moller-Jensen, J.
533 (2012). Escherichia coli uropathogenesis in vitro: invasion, cellular escape, and secondary
534 infection analyzed in a human bladder cell infection model. Infect Immun *80*, 1858-1867.
535 Antimicrobial Resistance, C. (2022). Global burden of bacterial antimicrobial resistance in
536 2019: a systematic analysis. Lancet *399*, 629-655.
537 Ballen, V., Ratia, C., Cepas, V., and Soto, S.M. (2020). Enterococcus faecalis inhibits Klebsiella
538 pneumoniae growth in polymicrobial biofilms in a glucose-enriched medium. Biofouling *36*,
539 846-861.
540 Balleza, E., Kim, J.M., and Cluzel, P. (2018). Systematic characterization of maturation time of
541 fluorescent proteins in living cells. Nature methods *15*, 47-51.
542 Beroz, F., Yan, J., Sabass, B., Stone, H.A., Bassler, B.L., Wingreen, N.S., and Meir, Y. (2018).
543 Verticalization of bacterial biofilms. Nat Phys *14*, 954-960.
544 Berry, R.E., Klumpp, D.J., and Schaeffer, A.J. (2009). Urothelial cultures support intracellular
545 bacterial community formation by uropathogenic Escherichia coli. Infect Immun *77*, 2762-
546 2772.
547 Billips, B.K., Forrestal, S.G., Rycyk, M.T., Johnson, J.R., Klumpp, D.J., and Schaeffer, A.J. (2007).
548 Modulation of host innate immune response in the bladder by uropathogenic Escherichia coli.
549 Infect Immun *75*, 5353-5360.
550 Billips, B.K., Schaeffer, A.J., and Klumpp, D.J. (2008). Molecular basis of uropathogenic
551 Escherichia coli evasion of the innate immune response in the bladder. Infect Immun *76*,
552 3891-3900.
553 Ch'ng, J.H., Chong, K.K.L., Lam, L.N., Wong, J.J., and Kline, K.A. (2019). Biofilm-associated
554 infection by enterococci. Nat Rev Microbiol *17*, 82-94.
555 Croxall, G., Weston, V., Joseph, S., Manning, G., Cheetham, P., and McNally, A. (2011).
556 Increased human pathogenic potential of Escherichia coli from polymicrobial urinary tract
557 infections in comparison to isolates from monomicrobial culture samples. J Med Microbiol *60*,
558 102-109.
559 de Vos, M.G.J., Zagorski, M., McNally, A., and Bollenbach, T. (2017). Interaction networks,
560 ecological stability, and collective antibiotic tolerance in polymicrobial infections. Proceedings
561 of the National Academy of Sciences of the United States of America *114*, 10666-10671.
562 Debroy, S., van der Hoeven, R., Singh, K.V., Gao, P., Harvey, B.R., Murray, B.E., and Garsin, D.A.
563 (2012). Development of a genomic site for gene integration and expression in Enterococcus
564 faecalis. J Microbiol Methods *90*, 1-8.
565 Desai, P.J., Pandit, D., Mathur, M., and Gogate, A. (2001). Prevalence, identification and
566 distribution of various species of enterococci isolated from clinical specimens with special
567 reference to urinary tract infection in catheterized patients. Indian J Med Microbiol *19*, 132-
568 137.
569 Ducret, A., Quardokus, E.M., and Brun, Y.V. (2016). MicrobeJ, a tool for high throughput
570 bacterial cell detection and quantitative analysis. Nat Microbiol *1*, 16077.
571 Duncan, M.J., Li, G., Shin, J.S., Carson, J.L., and Abraham, S.N. (2004). Bacterial penetration of
572 bladder epithelium through lipid rafts. J Biol Chem *279*, 18944-18951.
573 Eto, D.S., Jones, T.A., Sundsbak, J.L., and Mulvey, M.A. (2007). Integrin-mediated host cell
574 invasion by type 1-piliated uropathogenic Escherichia coli. PLoS pathogens *3*, e100.
575 Flemming, H.C., and Wingender, J. (2010). The biofilm matrix. Nat Rev Microbiol *8*, 623-633.

576 Flores-Mireles, A.L., Walker, J.N., Caparon, M., and Hultgren, S.J. (2015). Urinary tract
577 infections: epidemiology, mechanisms of infection and treatment options. Nat Rev Microbiol
578 *13*, 269-284.
579 Fourcade, C., Canini, L., Lavigne, J.P., and Sotto, A. (2015). A comparison of monomicrobial
580 versus polymicrobial Enterococcus faecalis bacteriuria in a French University Hospital. Eur J
581 Clin Microbiol Infect Dis *34*, 1667-1673.
582 Foxman, B. (2014). Urinary tract infection syndromes: occurrence, recurrence, bacteriology,
583 risk factors, and disease burden. Infect Dis Clin North Am *28*, 1-13.
584 Galvan, E.M., Mateyca, C., and Ielpi, L. (2016). Role of interspecies interactions in dual-species
585 biofilms developed in vitro by uropathogens isolated from polymicrobial urinary catheter-
586 associated bacteriuria. Biofouling *32*, 1067-1077.
587 Ganderton, L., Chawla, J., Winters, C., Wimpenny, J., and Stickler, D. (1992). Scanning electron
588 microscopy of bacterial biofilms on indwelling bladder catheters. Eur J Clin Microbiol Infect
589 Dis *11*, 789-796.
590 Garsin, D.A., Frank, K.L., Silanpaa, J., Ausubel, F.M., Hartke, A., Shankar, N., and Murray, B.E.
591 (2014). Pathogenesis and Models of Enterococcal Infection. In Enterococci: From Commensals
592 to Leading Causes of Drug Resistant Infection, M.S. Gilmore, D.B. Clewell, Y. Ike, and N.
593 Shankar, eds. (Boston).
594 Gaston, J.R., Johnson, A.O., Bair, K.L., White, A.N., and Armbruster, C.E. (2021). Polymicrobial
595 interactions in the urinary tract: is the enemy of my enemy my friend? Infect Immun.
596 Horsley, H., Malone-Lee, J., Holland, D., Tuz, M., Hibbert, A., Kelsey, M., Kupelian, A., and Rohn,
597 J.L. (2013). Enterococcus faecalis subverts and invades the host urothelium in patients with
598 chronic urinary tract infection. PLoS One *8*, e83637.
599 Iosifidis, G., and Duggin, I.G. (2020). Distinct Morphological Fates of Uropathogenic
600 Escherichia coli Intracellular Bacterial Communities: Dependency on Urine Composition and
601 pH. Infect Immun *88*.
602 Justice, S.S., Hung, C., Theriot, J.A., Fletcher, D.A., Anderson, G.G., Footer, M.J., and Hultgren,
603 S.J. (2004). Differentiation and developmental pathways of uropathogenic Escherichia coli in
604 urinary tract pathogenesis. Proceedings of the National Academy of Sciences of the United
605 States of America *101*, 1333-1338.
606 Justice, S.S., Hunstad, D.A., Seed, P.C., and Hultgren, S.J. (2006). Filamentation by Escherichia
607 coli subverts innate defenses during urinary tract infection. Proceedings of the National
608 Academy of Sciences of the United States of America *103*, 19884-19889.
609 Kau, A.L., Martin, S.M., Lyon, W., Hayes, E., Caparon, M.G., and Hultgren, S.J. (2005).
610 Enterococcus faecalis tropism for the kidneys in the urinary tract of C57BL/6J mice. Infect
611 Immun *73*, 2461-2468.
612 Klein, K., Palarasah, Y., Kolmos, H.J., Moller-Jensen, J., and Andersen, T.E. (2015).
613 Quantification of filamentation by uropathogenic Escherichia coli during experimental
614 bladder cell infection by using semi-automated image analysis. J Microbiol Methods *109*, 110-
615 116.
616 Klein, R.D., and Hultgren, S.J. (2020). Urinary tract infections: microbial pathogenesis, host-
617 pathogen interactions and new treatment strategies. Nat Rev Microbiol *18*, 211-226.
618 Kline, K.A., and Lewis, A.L. (2016). Gram-Positive Uropathogens, Polymicrobial Urinary Tract
619 Infection, and the Emerging Microbiota of the Urinary Tract. Microbiol Spectr *4*.
620 Klumpp, D.J., Weiser, A.C., Sengupta, S., Forrestal, S.G., Batler, R.A., and Schaeffer, A.J. (2001).
621 Uropathogenic Escherichia coli potentiates type 1 pilus-induced apoptosis by suppressing NF-
622 kappaB. Infect Immun *69*, 6689-6695.

623 Kucheria, R., Dasgupta, P., Sacks, S.H., Khan, M.S., and Sheerin, N.S. (2005). Urinary tract
624 infections: new insights into a common problem. Postgraduate Medical Journal *81*, 83-86.
625 Macleod, S.M., and Stickler, D.J. (2007). Species interactions in mixed-community crystalline
626 biofilms on urinary catheters. J Med Microbiol *56*, 1549-1557.
627 Martinez, J.J., Mulvey, M.A., Schilling, J.D., Pinkner, J.S., and Hultgren, S.J. (2000). Type 1 pilus-
628 mediated bacterial invasion of bladder epithelial cells. EMBO J *19*, 2803-2812.
629 Mulvey, M.A., Lopez-Boado, Y.S., Wilson, C.L., Roth, R., Parks, W.C., Heuser, J., and Hultgren,
630 S.J. (1998). Induction and evasion of host defenses by type 1-piliated uropathogenic
631 Escherichia coli. Science *282*, 1494-1497.
632 Mulvey, M.A., Schilling, J.D., and Hultgren, S.J. (2001). Establishment of a persistent
633 Escherichia coli reservoir during the acute phase of a bladder infection. Infect Immun *69*,
634 4572-4579.
635 Mysorekar, I.U., and Hultgren, S.J. (2006). Mechanisms of uropathogenic Escherichia coli
636 persistence and eradication from the urinary tract. Proceedings of the National Academy of
637 Sciences of the United States of America *103*, 14170-14175.
638 Prudent, V., Demarre, G., Vazeille, E., Wery, M., Quenech'Du, N., Ravet, A., Dauverd-Girault,
639 J., van Dijk, E., Bringer, M.A., Descrimes, M.*, et al.* (2021). The Crohn's disease-related
640 bacterial strain LF82 assembles biofilm-like communities to protect itself from
641 phagolysosomal attack. Commun Biol *4*, 627.
642 Qin, B., Fei, C., Bridges, A.A., Mashruwala, A.A., Stone, H.A., Wingreen, N.S., and Bassler, B.L.
643 (2020). Cell position fates and collective fountain flow in bacterial biofilms revealed by light-
644 sheet microscopy. Science *369*, 71-77.
645 Rosen, D.A., Hooton, T.M., Stamm, W.E., Humphrey, P.A., and Hultgren, S.J. (2007). Detection
646 of intracellular bacterial communities in human urinary tract infection. PLoS Med *4*, e329.
647 Rosen, D.A., Pinkner, J.S., Jones, J.M., Walker, J.N., Clegg, S., and Hultgren, S.J. (2008).
648 Utilization of an intracellular bacterial community pathway in Klebsiella pneumoniae urinary
649 tract infection and the effects of FimK on type 1 pilus expression. Infect Immun *76*, 3337-3345.
650 Sauer, M.M., Jakob, R.P., Eras, J., Baday, S., Eris, D., Navarra, G., Berneche, S., Ernst, B., Maier,
651 T., and Glockshuber, R. (2016). Catch-bond mechanism of the bacterial adhesin FimH. Nature
652 communications *7*, 10738.
653 Shah, C., Baral, R., Bartaula, B., and Shrestha, L.B. (2019). Virulence factors of uropathogenic
654 Escherichia coli (UPEC) and correlation with antimicrobial resistance. BMC Microbiol *19*, 204.
655 Shaner, N.C., Lin, M.Z., McKeown, M.R., Steinbach, P.A., Hazelwood, K.L., Davidson, M.W.,
656 and Tsien, R.Y. (2008). Improving the photostability of bright monomeric orange and red
657 fluorescent proteins. Nature methods *5*, 545-551.
658 Shankar, N., Lockatell, C.V., Baghdayan, A.S., Drachenberg, C., Gilmore, M.S., and Johnson,
659 D.E. (2001). Role of Enterococcus faecalis surface protein Esp in the pathogenesis of ascending
660 urinary tract infection. Infect Immun *69*, 4366-4372.
661 Söderström, B., Pittorino, M.J., Daley, D.O., and Duggin, I.G. (2022). Assembly dynamics of
662 FtsZ and DamX during infection-related filamentation and division in uropathogenic E. coli.
663 Nature communications *13*, 3648.
664 Song, J., Bishop, B.L., Li, G., Duncan, M.J., and Abraham, S.N. (2007). TLR4-initiated and cAMP-
665 mediated abrogation of bacterial invasion of the bladder. Cell Host Microbe *1*, 287-298.
666 Stickler, D.J. (2008). Bacterial biofilms in patients with indwelling urinary catheters. Nat Clin
667 Pract Urol *5*, 598-608.
668 Tandogdu, Z., Bartoletti, R., Cai, T., Cek, M., Grabe, M., Kulchavenya, E., Koves, B., Menon, V.,
669 Naber, K., Perepanova, T.*, et al.* (2016). Antimicrobial resistance in urosepsis: outcomes from

670 the multinational, multicenter global prevalence of infections in urology (GPIU) study 2003-
671 2013. World J Urol *34*, 1193-1200.
672 Tien, B.Y.Q., Goh, H.M.S., Chong, K.K.L., Bhaduri-Tagore, S., Holec, S., Dress, R., Ginhoux, F.,
673 Ingersoll, M.A., Williams, R.B.H., and Kline, K.A. (2017). Enterococcus faecalis Promotes Innate
674 Immune Suppression and Polymicrobial Catheter-Associated Urinary Tract Infection. Infect
675 Immun *85*.
676 Wang, X., Lünsdorf, H., Ehrén, I., Brauner, A., and Römling, U. (2010). Characteristics of
677 biofilms from urinary tract catheters and presence of biofilm-related components in
678 Escherichia coli. Curr Microbiol *60*, 446-453.
679 Watson, J.F., and Garcia-Nafria, J. (2019). In vivo DNA assembly using common laboratory
680 bacteria: A re-emerging tool to simplify molecular cloning. J Biol Chem *294*, 15271-15281.
681 Wright, K., de Silva, K., Plain, K.M., Purdie, A.C., Blair, T.A., Duggin, I.G., Britton, W.J., and
682 Oehlers, S.H. (2021). Mycobacterial infection-induced miR-206 inhibits protective neutrophil
683 recruitment via the CXCL12/CXCR4 signalling axis. PLoS pathogens *17*, e1009186.
684 Xia, L., Liu, Y., Xia, S., Kudinha, T., Xiao, S.N., Zhong, N.S., Ren, G.S., and Zhuo, C. (2017).
685 Prevalence of ST1193 clone and IncI1/ST16 plasmid in E-coli isolates carrying bla(CTX-M-55)
686 gene from urinary tract infections patients in China. Scientific reports *7*, 44866.
687 Yan, J., Sharo, A.G., Stone, H.A., Wingreen, N.S., and Bassler, B.L. (2016). Vibrio cholerae
688 biofilm growth program and architecture revealed by single-cell live imaging. Proceedings of
689 the National Academy of Sciences of the United States of America *113*, E5337-5343.
690 Zhu Tan, C.A., Lam, L.N., Biukovic, G., Soh, E.Y.-C., Toh, X.W., Lemos, J.A., and Kline, K.A. (2022).
691 Enterococcus faecalis antagonizes Pseudomonas aeruginosa growth in polymicrobial biofilms.
692 bioRxiv, 2022.2001.2018.476859.
693